# Chapter 2
# Fabrication Methods of Artificial Microstructures

## 2.1 Metallic Glass (MG) Alloy Synthesis

The exceptional processability and large supercooled liquid region (SCLR) of MGs makes them highly promising candidates for thermoplastic processing, especially when replicating features with high precision and tolerance. A lightweight $Zr_{35}Ti_{30}Cu_{7.5}Be_{27.5}$ MG former ($\rho \approx 3.9$ g cm$^{-3}$), which has the largest SCLR of $\Delta T = 159$ K (at 20 K/min heating rate) of any known bulk glass forming alloy is utilized for heterostructure fabrication. This alloy can be cast into fully amorphous rods of 1.5 cm in diameter, and shows enhanced glass forming ability (GFA). In addition, this alloy exhibits high-yield strength in compression ($\sigma_y = 1430$ GPa) and relatively better fracture toughness than many other MGs, and a relatively high Poisson's ratio of $v = 0.37$. The undercooled liquid exhibits an unexpectedly high Angell Fragility of $m = 65.6$ [1]. Microreplication methods carried out in open air using relatively low applied pressures (~1 atm) demonstrate superior thermoplastic processability of Zr-based alloys for engineering applications [2]. Furthermore, strain rate effects on viscosity of this alloy and similar Zr-based MG alloys have been extensively studied [1, 3], and based on these measurements, it is demonstrated that $Zr_{35}Ti_{30}Cu_{7.5}Be_{27.5}$ exhibits exceptional properties for thermoplastic processing.

To cast, the weight percent's for the constituent elements were calculated, and each element was separately measured three times with a calibrated balance. The constituents were subsequently mixed in a quartz tube in a Ti-gettered argon atmosphere under vacuum, and melted with purity higher than 99.99 % in an arc melter, which was subsequently cooled down in air. This process forms a homogenous crystalline ingot. In order to prepare amorphous samples, the cast ingot was sealed in a quartz tube under vacuum of $10^{-6}$ mbar, and the quartz tube was subsequently purged with an inert gas several times to eliminate any residual oxygen content. The ingot was then heated above its liquidus temperature for 5 min, and quenched in water respectively, which results in a rod-shaped MG [2].

In addition, $Pt_{57.5}Cu_{14.7}Ni_{5.3}P_{22.5}$ MG with a low TPF processing temperature (~250−280 °C) and outstanding formability was used [4]. Its processing temperature is lower than the melting point of most metals, and has very high corrosion



B. Sarac, *Microstructure-Property Optimization in Metallic Glasses*, Springer Theses,
DOI 10.1007/978-3-319-13033-0_2

and wear resistance. The glass transition and crystallization temperatures for the $Pt_{57.5}Cu_{14.7}Ni_{5.3}P_{22.5}$ MG are 230 and 310 °C, respectively, indicating a large processing window [5]. Extensive plasticity was observed during bending and unconfined uniaxial compression, and is a consequence of the very large Poisson ratio ($\nu = 0.42$) of the material [4].

Pt-MG ingot was prepared by melting the elements of purity better than 99.99 % in a vacuum-sealed quartz tube. $B_2O_3$ was used to flux the ingot for 15 min, which was shown to increase the GFA by reducing the alloy's oxides. An amorphous rod was obtained by casting it in a quartz tube, and by subsequent water quenching. X-ray diffraction machine (XRD-6000 Shimadzu) and differential scanning calorimeter (DSC; Perkin Elmer Diamond DSC) confirmed that both MG formers are fully amorphous [2].

## 2.2 Silicon Mold Fabrication

Honeycomb features were designed using AutoCAD 2011 software program. Overall, a circular area of 15 cm in diameter (150 mm Si wafer) can be covered with patterned molds of the artificial microstructures. Figure 2.1 shows the schematics of the CAD drawing of various honeycomb patterns designed. The drawing layout was transferred to a photomask maker (Heidelberg DWL-66 Laser Mask Writer), which uses direct laser beam writing to fabricate the chromium-etching mask. A

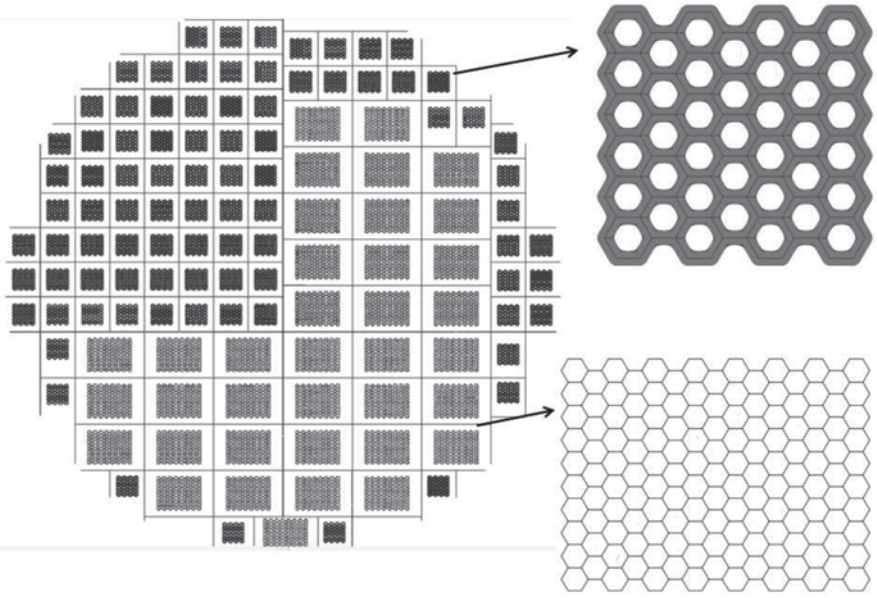

**Fig. 2.1** CAD drawing of various cellular structures designed for 6″ (150 mm) wafer

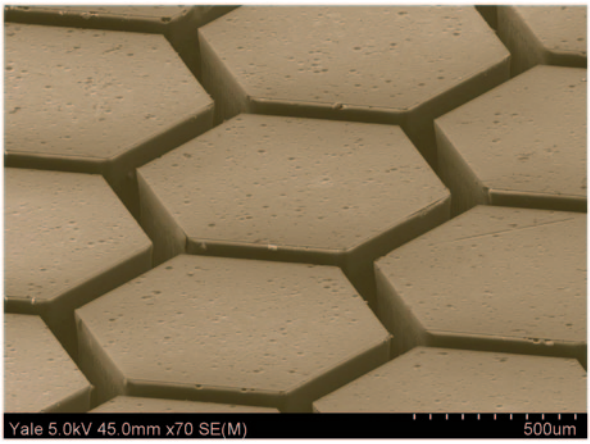


**Fig. 2.2** Negative Si template of a honeycomb structure fabricated by deep reactive ion etching (DRIE) process. High precision on the etched lateral walls, as well as on the edges of the features can be obtained, which is subsequently be replicated precisely by metallic glasses (MGs). Pitting is observed only on the outer surface of the mold, which is due to the overexposure of the photoresist required for high-aspect ratio etches

layer of AZ P4620 photoresist was deposited onto the silicon wafer at a speed of 3000 rpm for 42 s, which was successively patterned using basic photolithography. The final thickness of the coating was 8 μm. After the deposition of the photoresist, deep reactive ion etching (DRIE) method was utilized to each exposed areas of Si wafer. DRIE processing etch cycle was performed under 12 s, 130-sccm $SF_6$, 13-sccm $O_2$, 600-W coil power, 12-W platen power, and 26-mtorr pressure, and the passivation cycle was performed under 8 s, 85-sccm $C_4F_8$, 600-W coil power, 0-W platen power, and 15-mtorr pressure. The etching depth of the honeycomb molds was measured to be around $300 \pm 30$ μm, where the etching depth of the cellular structure molds was controlled through the etching time. The etched samples were diced using a wafer-dicing saw. The excessive resist layer was then removed from the surface by cleaning in acetone, isopropanol, and deionized water, respectively. $N_2$ was used to dry the Si wafer under a pressure of $2 \times 10^5$ Pa. Figure 2.2 shows an example of a honeycomb Si mold pattern with 100 μm wide feature size. It is important to note that lateral spacing of about 2 mm between the molds was kept to prevent stress concentrations between the samples during the fabrication of the Si mold.

## 2.3 Fabrication Methods of MG Artificial Microstructures

Novel TPF-based processing methods developed for MGs have remarkably increased the possibility of geometries that can be net shaped [6]. To exemplify, complex shapes that were previously unachievable with any metal processing method can be easily fabricated with high precision using this concept [7, 8]. A considerable attention has lately been given to the TPF of MGs on micro- and nanoscale applica-

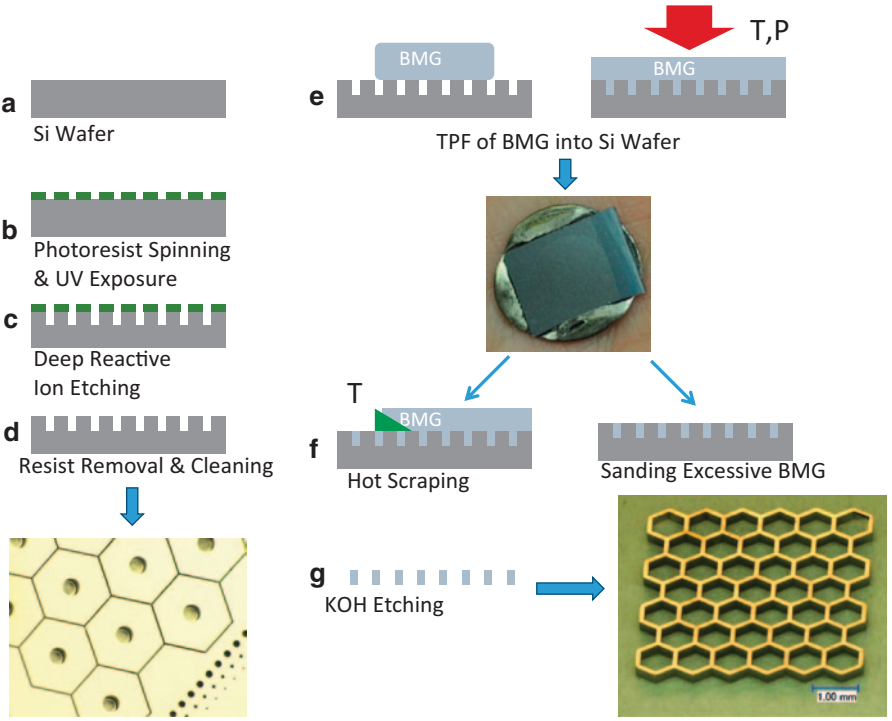


**Fig. 2.3** Schematics of the MG cellular structure fabrication. **a** Silicon is used as a mold material. **b** A thin layer of photoresist on the *Si wafer* is patterned by UV exposure through a mask. **c** The exposed regions of the *Si wafer* are etched by *deep reactive ion etching* (DRIE). **d** The residual photoresist is removed. **e** The etched *Si wafer*, containing the cellular structure features, are filled with Zr- or Pt-MG by TPF based compression molding. **f** Residual MG is either removed by *hot scraping* or polishing. **g** The cellular structure of 39 cells is released by etching the *Si wafer* in KOH (Reprinted from reference [20] with a permission from John Wiley and Sons)

tions due to their homogeneous structure and ease in fabrication on multiple length scales [9–17].

We consider $Zr_{35}Ti_{30}Cu_{7.5}Be_{27.5}$ as a typical MG with negligible macroscopic plasticity [1] and, as a comparison, $Pt57.5Cu_{14.7}Ni_{5.3}P_{22.5}$, which exhibits unusually high, ~20 % compressive plasticity in their bulk forms [4]. Both alloys are well suited for the TPF fabrication of the cellular structures due to their high formability [5].

Figure 2.3 shows the fabrication steps of the MG cellular structures. Discs of 1 mm thickness cut from the amorphous MG rods were pre-pressed to a thickness of around 500 μm by using Instron 5569 tensile testing machine (50 kN maximum load capacity) via compression plates. The Si mold containing the desired pattern was heated to the TPF temperature of the related MG, and the pre-pressed MG disc was placed on the heated mold and equilibrated to attain a stable temperature. The cellular structures were produced by thermoplastic compression molding of $Zr_{35}Ti_{30}Cu_{7.5}Be_{27.5}$ at 425 and 275 °C for $Pt_{57.5}Cu_{14.7}Ni_{5.3}P_{22.5}$ in air into the etched

Si mold for 60 s under a pressure of 50 MPa. Under these conditions, the MG subsequently relaxes into a highly viscous metastable liquid, and flows into the etched mold under controlled pressure [18]. The TPF processing temperature is selected on the basis of the viscosity change as a function of temperature and processing window. A typical temperature used for TPF is chosen such that the viscosity decreases to $10^6$–$10^8$ Pa·s as the crystallization time is approximately 3–5 min [19]. Air-cooling is sufficient to preserve its amorphous nature, which can be verified by subsequent thermal and structural analysis. The key to TPF-based compression molding is the precise temperature control, and the applied pressure should exceed the flow stress of the MG to achieve the required strain before crystallization sets in. As the viscosity of the MG in its supercooled liquid state changes by roughly an order of magnitude per every 20 °C, temperature fluctuations during net-shaping should be minimized [19].

After the pressed samples were cooled down to room temperature, the extra MG layer was removed by either hot cutting [12] at 390 °C or by polishing using Buehler Metaserv 250 Grinder-Polisher. The aspect ratio dependent etching rate of Si molds results in cellular structures varying in depth. Samples were grinded down to 200 ± 10 μm to have uniformity in depth (z-direction) of the MG cellular structures with different *l*/*t* ratio. The MG cellular structure comprised of 39 cells was subsequently released from the mold by etching the Si mold in KOH for 30 min at 100°C (Fig. 2.3g). The fully amorphous structure was confirmed by subsequent thermal and structural analysis. Similarly, MG heterostructures for tensile testing were also created using this twofold technique, where the precision of the CAD drawing can be translated into the MG within a precision of a micron (Fig 2.4).

Thermoplastic forming (TF) of MGs into Si molds causes residual stresses at the matrix-second phase interface due to the linear expansion coefficient difference between the Si pillars and the MG surrounding them. Tensile heterostructures were subsequently postannealed at 380 °C for 5 min (processing window at this temperature measured by the differential scanning calorimeter is ~20 min) to dissipate the stress concentrations caused from the fabrication step. Surface oxidation caused by the postannealing process was eliminated by polishing the surface of the sample. Using this pretest method, overall fracture strength and strain of MG heterostructures improved by ~10 %, and this increase is accounted for the linear expansion of the pores through:

$$\sigma_{xx} = E(x)\alpha(x)\Delta T \tag{2.1}$$

where $E$ (elastic modulus of the heterostructure) is taken as 20 GPa for a porous sample, $\alpha$ (linear expansion coefficient) is taken as $10^{-5}$ 1/K [21], and the temperature difference as 400 K, which results in $\sigma_{xx} = \sigma_{yy} = 80$ MPa.

The net-shaping of thin parts of MGs is restricted by friction between the mold and the viscous MG. An ideal method to eliminate friction is blow molding, which has been demonstrated for MGs on the macroscale [7]. Using this unique shaping method, it has been already shown that the formation of precise net shaping of

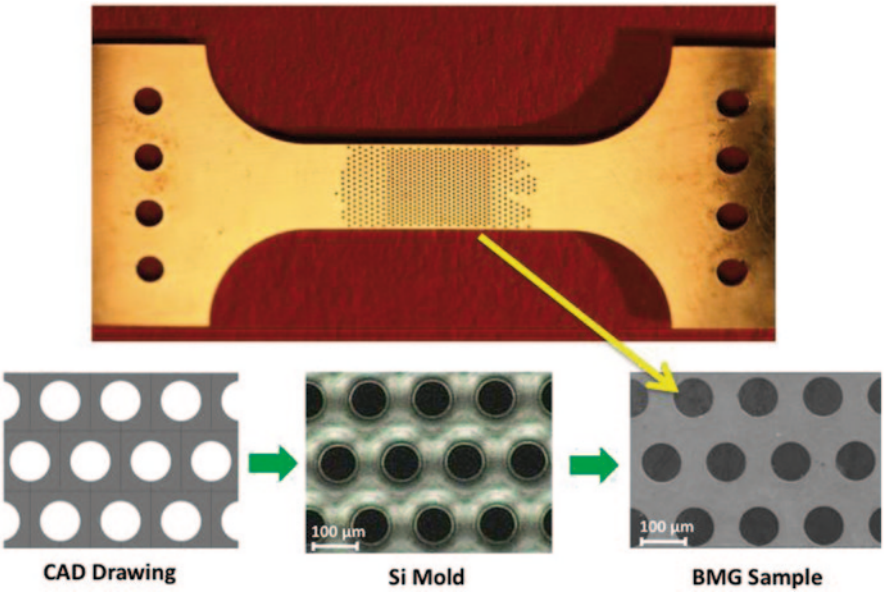


**Fig. 2.4** MG heterostructure realized in a tensile test sample, and close-up image of its gauge section. Comparison of the *Si-mold* with the original *CAD drawing* reveals the control and precision of our process

complex parts over a wide range of length scales (from angstrom to meter-scale) is possible [22]. To show the experimental feasibility of the blow-molding process, our group has utilized a free-expansion technique [2]. A schematic sketch of the blow molding of 3D microshells at its processing conditions is shown in Fig. 2.5(i). The side and cross-sectional view of a blow molded MG microshell is shown in Fig. 2.5(ii-a, b). The uniformity of the shells in Fig. 2.5(ii-c) suggests that the expansion process can be well controlled on a macroscale. MGs feature the largest resistance to thinning at typical blow molding conditions, and hence, the cross-sectional profile has a very high uniformity [5]. Figure 2.5(iii) depicts the change in aspect ratio ($h/d_0$) during expansion as a function of temperature. A large and desired processing window is available for blow molding a hollow shape with an aspect ratio of 2 at 450 °C and above.

In addition, our group has presented a method to fabricate 3D $Pt_{57.5}Cu_{14.7}Ni_{5.3}P_{22.5}$ MG microshells attached to a Si wafer by combining TPF-based blow molding and compression molding of MG. The details of the Si mold photolithography, measures taken to protect the MG disc from flowing into the big cavities, and the TPF based compression molding are delineated in [2]. In this method, the MG-Si assembly is brought to the processing temperature of 275 °C. As a result, the unsupported MG diaphragm expands into a 3D shell while attached to the Si wafer at the same time (Fig. 2.5(iv-a, b). The height of the MG shells can be adjusted

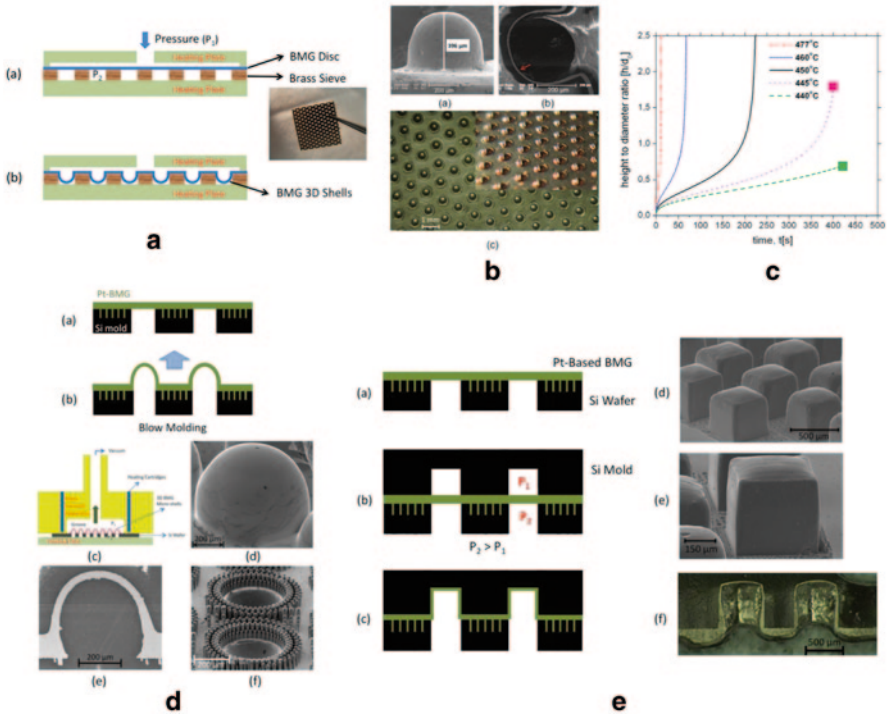


**Fig. 2.5** (*i*) The $Zr_{44}Ti_{11}Ni_{10}Cu_{10}Be_{25}$ MG disc and brass sieve are gradually heated to the processing temperature of the MG of 450 °C. For blow molding, $\Delta P = 10^5$ Pa pressure difference is generated between the top and the bottom sides of the disk by applying pressure of $2 \times 10^5$ Pa to the top of the disc. (*ii*) **a** A side view and **b** 90° rotated cross-sectional view of a MG microshell taken by SEM. (**c** and inset) Array of microshells produced by blow molding through a brass sieve with 500 μm holes. (*iii*) Expansion kinetics of a $Zr_{44}Ti_{11}Cu_{10}Ni_{10}Be_{25}$ shell at various temperatures under a pressure difference of $5 \times 10^5$ Pa with a template feature diameter and initial disc thickness of 500 and 200 μm, respectively. The onset of crystallization is indicated by the solid squares which terminates the expansion. Change in the height of the 3D shell with respect to blowing time is used to estimate the expansion kinetics. (*iv*) **a**-**b** The pressed Pt-MG layer is blow molded through large holes where the filled small holes anchor the Pt-based MG to the Si wafer. **c** The vacuum apparatus applies a pressure gradient ($P_1 < P_2$) of 0.1 atm between the front and the backside of the MG-Si assembly. **d** A side view of a ~500 μm microshell, **e** a cross-sectional view, and **f** the MG side that is originally attached to the Si wafer is depicted. Pt57.5Cu14.7Ni5.3P22.5 is blow molded into a square mold at 275 °C for 30 s at a pressure difference of 5 t 105 Pa

by optimizing temperature, time, and pressure (see Fig. 2.5(iii)). Uniform stress distribution inside the diaphragm ensures the sphericity of MGs shells, which mainly depends on the thickness of the initial MG layer. A schematic sketch of the vacuum setup is presented in Fig. 2.5(iv-c), which was used to blow mold 3D microshells. Si seals the groove of the vacuum apparatus inserted on top of the MG-Si assembly. Figure 2.5(iv-d) shows the freely expanded Pt-based MG

shell by blow molding. The Si wafer was subsequently etched using KOH to visualize the attachment of the microshells to Si via the small anchoring holes. Figure 2.5(iv-e) is the cross-sectional view of the expanded shell, where the microshell has ~40 μm thickness at the pole. SEM image of the MG side is illustrated in Fig. 2.5(iv-f), which was originally attached to the Si wafer. A strong attachment of the MG to the Si wafer is provided by the DRIE process, which produces the vertical surface roughness (scalloping effect) of ~400 nm.

The 3D shell fabrication method can also generate shells beyond the free expanded spherical shapes by blowing into mold cavities ([2]; Fig. 2.5(v)). In this technique, a second Si wafer with square cavities (500 μm each side) is used as a template. $Pt_{57.5}Cu_{14.7}Ni_{5.3}P_{22.5}$ is attached to a Si wafer using similar conditions in Fig. 2.5(iv). A second Si mold with the square cavities of the same dimensions is clamped to the MG-Si assembly and aligned with reference to the larger cavities in the original Si wafer (Fig. 2.5(v-b)). Argon gas is utilized to create a pressure difference between two sides under inert environment, which blows the attached MG into the square mold cavities (Fig. 2.5c). Fig. 2.5(v-d, e) show examples of square MG shells anchored to Si wafer. The pole section of the blow-molded shells are ~15 μm (Fig. 2.5(v-f)). This novel production technique corroborates that MG shells with controlled shapes can be created with high precision and throughput.

## Conclusions

In this chapter, TPF was introduced as a net-shape processing method for MGs, which decouples fast cooling and forming processes. TPF is a highly robust and versatile shaping method, and it is very similar to the techniques used for processing thermoplastics. Table 2.1 summarizes the wide range of TPF methods compared to conventional casting [22]. Due to the versatility and high precision, TPF process is ideal for replicating small features and thin sections with high aspect ratios, which makes this process appropriate for microelectromechanical systems (microfluidic devices, microthrusters), nano- and microtechnology (resonators, acoustic transducers, packaging, microlenses, and microvalves), jewelry, biomedical (superelastic springs, stents, neural impulse actuators) and optical applications, and data storage. Furthermore, highly spherical 3D shells created by blow molding with controlled roughness of less than 2 nm grants MGs an inherently high Q-factor for resonator applications, as well as for microelectromechanical systems (MEMS) or complementary metal-oxide semiconductor (CMOS) devices [2].

**Table 2.1** Process-selection map for generic shapes that can be fabricated with various TPF-based MG fabrication methods (Reprinted from [22] reference with a permission from John Wiley and Sons)

| Process | Process based on | Shape/ Size | Shape/ Aspect ratio | Shape/ Feature | Process level of maturity | BMC former used | Surface finish | Dimensional accuracy | Issues/Comment |
|---|---|---|---|---|---|---|---|---|---|
| Compression molding; Injection molding | TPF | Millimeters to centimeters | 1–10 | Undercuts open | R&D medium | $Zr_{44}Ti_{11}Cu_{10}Ni_{10}Be_{25}$ [81,82] $Pd_{40}Ni_{10}Cu_{30}P_{20}$ [117] $Zr_{35}Ti_{30}Be_{27.5}Cu_{7.5}$ [292] | Very good | Good | Mold release; mold wear due to high required forming pressures can be combined with surface patterning <1 μm |
| Blow molding | TPF | 10 μm to centimeters (10+) | 10–1000 | Hollow, undercuts; low symmetry | R&D high | $Zr_{44}Ti_{11}Cu_{10}Ni_{10}Be_{25}$ [286] $Pt_{57.5}Cu_{14.7}Ni_{5.3}P_{22.5}$ [291] $Au_{49}Ag_{5.5}Pd_{2.3}Cu_{26.9}Si_{16.3}$ [291] $Zr_{35}Ti_{30}Be_{27.5}Cu_{7\cdot5}$ [291] $Zr_{53}Ti_{5}Cu_{20}Ni10Al_{12}$ [240] $Zr_{65}Al_{10}Ni_{10}Cu_{15}$ [364] | Excellent | Excellent | Most versatile shapes possible. Can be combined with joining and surface patterning < 10 μm. Size is limited by the maximum casting thickness of preshape only |
| Hot-rolling | TPF | Millimeters to centimeters (10+) | 100+ | Sheets | R&D low | $Zr_{44}Ti_{11}Cu_{10}Ni_{10}Be_{25}$ [285] | Good | Moderately good | Temperature-control critical; aspect ratio and shape size can be increased to ∞ in a continuous process |

**Table 2.1** (continued)

| Process | Process based on | Shape/ Size | Shape/ Aspect ratio | Shape/ Feature | Process level of maturity | BMC former used | Surface finish | Dimensional accuracy | Issues/Comment |
|---|---|---|---|---|---|---|---|---|---|
| Extrusion | TPF | Millimeters to meters | 100 | Long fixed cross-sectional profile, hollow | R&D low | CuTiZrNi [326,327,329] $Mg_{85}Y_{10}Cu_5$ [410] $Zr_{41.2}Ti_{13.8}Cu_{12.5}Ni_{10}Be_{22.5}$ [411] $Zr_{65}Al_{10}Ni_{10}Cu_{15}$ [323] $Ti_{50}Cu_{18}Ni_{22}Al_4Sn_6$ [412] $Mg_{5.8}Cu_{31}Y_6$ [413] $Zr_{44}Ti_{11}Cu_{10}Ni_{10}Be_{25}$ [333] | Good | Moderate | Swelling ~ 15% has to be considered; Sharp corners round off |
| Microimprinting (miniature imprinting, hot-embossing) | TPF | Micrometers to millimeters | 1–10 | Surface patterning | R&D industrialization | $La_{55}Al_{25}Ni_{20}$ [414] $Pt_{48.75}Pd_{9.75}Cu_{19.5}P_{22}$ [298,415] Zr-Al-Cu-Ni [296,416,417] $Zr_{44}Ti_{11}Cu_{10}Ni_{10}Be_{25}$ [245,418,419] $Pt_{57.5}Cu_{14.7}Ni_{5.3}P_{22.5}$ [245] Mg-Cu-Y [313] $Au_{49}Ag_{5.5}Pd_{2.3}Cu_{26.9}Si_{16.3}$ [245] $Zr_{41.2}Ti_{13.8}Cu_{12.5}Ni_{10}Be_{22.5}$ [302] $Zr_{46.8}Ti_{8.2}Cu_{7.5}Ni_{10}Be_{27.5}$ [420] $Pd_{40}Ni_{40}P_{20}$ [303,418] $Ce_{68}Al_{10}Cu_{20}Nb_2$ [50] | Very good | Good | Typically disposable molds; can also be combined with compression molding, hot-rolling, injection molding, and blow molding |
| Miniature manipulation | TPF | Nanometers to millimeters | ~ 1 | | R&D low | $Pd_{76}Cu_7Si_{17}$ [289,421] $Zr_{44}Ti_{11}Cu_{10}Ni_{10}Be_{25}$ [245] $Pt_{57.5}Cu_{14.7}Ni_{5.3}P_{22.5}$ [245,295,422] $Au_{49}Ag_{5.5}Pd_{2.3}Cu_{26.9}Si_{16.3}$ [245] | | | Bending, scrapping, smoothening |

http://www.springer.com/978-3-319-13032-3

Microstructure-Property Optimization in Metallic Glasses

Sarac, B.

2015, XIII, 89 p. 61 illus., 55 illus. in color., Hardcover
ISBN: 978-3-319-13032-3